Acta Biomaterialia 165 (2023) 72–85

Contents lists available at ScienceDirect

Acta Biomaterialia

journal homepage: www.elsevier.com/locate/actbio

Full length article

Hybrid spheroid microscaffolds as modular tissue units to build macro-tissue assemblies for tissue engineering☆

Olivier Guillaume[a,b], Oliver Kopinski-Grünwald[a,b], Gregor Weisgrab[a,b], Theresia Baumgartner[a], Aysu Arslan[c], Karin Whitmore[d], Sandra Van Vlierberghe[c], Aleksandr Ovsianikov[a,b,*]

[a] 3D Printing and Biofabrication Group, Institute of Materials Science and Technology, TU Wien (Technische Universität Wien), Getreidemarkt 9/308, Vienna 1060, Austria
[b] Austrian Cluster for Tissue Regeneration (http://www.tissue-regeneration.at), Austria
[c] Polymer Chemistry and Biomaterials Group, Centre of Macromolecular Chemistry, Department of Organic and Macromolecular Chemistry, Ghent University, Belgium
[d] University Service Center for Transmission Electron Microscopy, TU Wien, Austria

ARTICLE INFO

Article history:
Received 13 October 2021
Revised 2 March 2022
Accepted 7 March 2022
Available online 12 March 2022

Keywords:
Microscaffold
Stem cells
Two-photon polymerization
Spheroids
Third tissue engineering strategy
High-resolution 3D printing

ABSTRACT

Since its inception, tissue engineering and regenerative medicine (TERM) has been relying on either scaffold-based or scaffold-free strategies. Recent reports outlined the possibility of a synergistic, convergence approach, referred to as the third TERM strategy, which could alleviate bottlenecks of the two previous options. This strategy requires the fabrication of highly porous microscaffolds, allowing to create single spheroids within each of them. The resulting tissue units can then be combined and used as modular building blocks for creating tissue constructs through a bottom-up self-assembly. Such strategy can have a significant impact for the future of TERM, but so far, no reports have assessed its feasibility in detail.

This work reports a first systematic study, which includes a comparison of the *in vitro* behavior of tissue units based on adipose derived stem cell spheroids cultured within microscaffolds *versus* conventional spheroids. We first proved that the presence of the microscaffold neither impairs the cells 'ability to form spheroids nor impacts their viability. Importantly, the fusiogenic and the differentiation potential (i.e. chondrogenesis and osteogenesis), which are important features for cellularized building blocks to be used in TERM, are preserved when spheroids are cultured within microscaffolds. Significant benefits of microscaffold-based tissue units include the enhanced cell retention, the decreased compaction and the better control over the size observed when larger tissue constructs are formed through self-assembly.

The proof of concept study presented here demonstrates the great potential offered by those microsize tissue units to be used as building blocks for directed tissue self-assembly.

Statement of significance

One of the most exciting and recent advances in tissue engineering and regenerative medicine (TERM) is to combine together multiple micro-size cellularized units, which are able to self-assemble altogether to recreate larger tissue constructs.

In this work, we produce such modules by forming single spheroids within highly porous microscaffolds, and study how this new microenvironment impacts on the spheroid's behavior and stemness potential.

This work highlights as well that such novel route is enabled by two-photon polymerization, which is an additive manufacturing technique offering high spatial resolution down to 100 nm.

☆ Part of the Special Issue on Biofabrication with Spheroid and Organoid Materials, guest-edited by Professors Mark Skylar-Scott, Heidi Declercq, and Koichi Nakayama.

* Corresponding author at: 3D Printing and Biofabrication Group, Institute of Materials Science and Technology, TU Wien (Technische Universität Wien), Getreidemarkt 9/308, Vienna 1060, Austria.
E-mail address: aleksandr.ovsianikov@tuwien.ac.at (A. Ovsianikov).

https://doi.org/10.1016/j.actbio.2022.03.010

These findings provide a first scientific evidence about the utilization of hybrid spheroid microscaffold-based tissue units with great perspective as a modular tool for TERM.

1. Introduction

Tissue engineering and regenerative medicine (TERM) aims to restore, replace or regenerate tissues and organs through a multidisciplinary approach. Despite intense efforts, substantial challenges remain when fabricating large size tissues with high cellularity. The current TERM methods can be principally subdivided into scaffold-based or scaffold-free strategies [1,2]. For the scaffold-based approach, plethora of scaffolds have been proposed, which functions are basically to temporarily support the cell adhesion, proliferation and extracellular matrix (ECM) deposition; with the basic idea that the degradation kinetic of this engineered template will match the neo-tissue formation [3]. Obtaining *in vitro* constructs with a high cell density remains one of the main challenges of this approach [4]. The second approach, to which more and more importance is given, is the scaffold-free strategy [5,6]. This strategy can, for instance, involve spheroids, rather than single cell suspensions [7,8]. Indeed, it is now well acknowledged that 3D spheroids mimic *in vivo* cell behaviour and biological functionality better compared to 2D cellular monolayers [9]. Spheroids, which are dense cellular aggregates, overcome many current limitations existing when transplanting individual cells. For instance, injecting spheroids rather than a single cell suspension has been associated with better cell survival, increased cell retention and enhanced functionality in several preclinical trials [10–13].

Another appealing aspect when using spheroids is the possibility to use them as building blocks (modular tissue units), ideal for the bottom-up TERM strategy [2,14–16]. Indeed, when placed close to each other, spheroid units can merge to create one single body (in a process called fusiogenesis). Such directed tissue assembly is a recent and promising approach that provides enhanced level of control to organize building blocks into desired patterns that may then form a larger, macro-sized tissue [17,18]. Nevertheless, using only cellular spheroids as building blocks, in comparison to a robust scaffold, imposes intrinsic restrictions as the cells are not protected to any mechanical damage that can occur during handling or after deposition inside the body. The difficulty to have an engineered tissue with defined and controlled geometry is another recurrent and major issue when using bare spheroids as building blocks, due to fusion of the spheroid bodies and the naturally-occurring compaction of the final assembly [19–23]. Physically stabilizing the spheroids by placing them, one-by-one, on a microneedle array was proposed in a method called “Kenzan”. This method, however, restricts the tissue’s 3D design and requires a sophisticated robotic bioprinter [24,25].

A further bottom-up solution to engineering macro-sized tissues was shown through the directed assembly of small and biomimetic repeating units composed of, for instance, cell-laden hydrogels (i.e. microgels) [26–30]. However, as embedding cells into microgels severely limits the cell-cell interaction, the units lose the ability to self-assemble into a larger construct. Consequently, the aggregation of those building blocks into a larger tissue requires a complex work-flow, such as emulsification, physical packing or chemical crosslinking [31]. Translating this strategy to clinical scenario seems complicated due to those external manipulation steps. Indeed, in an ideal scenario, multiple micro-sized building blocks should be rapidly produced and then injected into the damaged tissue to fill up the defect, to self-assemble *in situ* and to mature in order to reconstitute the organ.

Examples of micro-sized units made of polymeric blocks instead of microgels were reported by Leferink et al. [32,33]. By incubating those “micro-objects” with cell suspension, macro-tissue assemblies could be formed through cell-cell and cell-ECM interaction. Still, the major bottleneck was that the degree of cellularity is significantly lower (compared to spheroids for instance), as those polymeric blocks are non-porous. Furthermore, the host cells colonized only the surfaces of those blocks. Creating highly porous microscaffolds capable of carrying complete spheroids would alleviate this bottleneck [4].

Several reports have demonstrated that highly porous cage-like microscaffolds, such as buckyballs (BB), can not only carry cells [34,35], but also support the formation of spheroids in their core [36,37]. This emerging approach called “third strategy for TERM” differs substantially from conventional scaffold-based and scaffold-free options [4]. As such, it integrates cellular spheroids cultured individually within robust microscaffolds, and consequently offers a synergism between both previous strategies.

The scope of this publication is to provide a systematic and comparative study between normal spheroids (SPH) and buckyball-based tissue units (BB) to better comprehend how stem cells behave in such hybrid cellular-polymer spheroids, in terms of proliferation, viability, shape-retention, fusion and differentiation.

Using human adipose-derived stem cells (hASCs), our *in vitro* data suggests that, when an appropriate design and porosity is selected, cellular spheroids can form within the microscaffolds. The shape of the resulting tissue unit is dictated by the microscaffold, meaning that the resulting multicellular bodies are then not necessarily spherical. We then verified that the presence of the microscaffold does not impair the viability of the cells, nor their differentiation potential. Both SPH and BB exhibit comparable fusiogenic ability and large-size tissue constructs can be formed via self-assembly when multiple units are incubated together. Compared to SPH, a significant advantage of using BB as building blocks is that the compaction of the resulting tissue is reduced, it is more stable over time and more controllable in terms of size.

These features are beneficial for the development of patient-specific spheroid-based therapy, where a defined tissue defect volume can then be filled by a matching volume of injectable BBs, which will then self-assemble into a stable tissue. This work underlines new opportunities in building tissues through the bottom-up approach using BB-based tissue units, having potential to overcome major current bottlenecks in the field of TERM.

2. Material and methods

2.1. Producing microscaffolds by two-photon polymerization (2PP)

For the current study, a commercially available biodegradable PCL-based resin (Degrad INX) was obtained from BIO INX (Ghent, Belgium). The photo-reactive resin was dispensed into the sample holders. These consisted of aluminum plates (25 mm × 75 mm × 3 mm) with quadratic openings (12 mm side length). One side of the opening was covered with a glass cover slip and sealed using a 2-component glue. The temperature of the resin was brought to 50 °C just prior starting the 2PP printing.

Polymerization was initiated by a femtosecond-pulsed laser (MaiTai eHP DeepSee, Spectra-Physics) operated at a wavelength of 800 nm, a repetition rate of 80 MHz and a pulse duration of 70 fs after the microscope objective (UPlanSApo, 10x/0.4 NA, Olympus, Japan). A microscope stage (ScanPLUS IM, 120 × 180, Märzhäuser-Wetzlar, Germany) was implemented to position the sample and a dual-axis galvanometric scanner (Scanlabs, Germany) was used to position the laser beam within the field of view. The system was controlled by a Think3D software from UpNano GmbH (https://www.upnano.at/software). The optimal printing parameters were screened by varying laser power (from 20 to 300 mW), line distance (hatch, from 0.5 to 2.5 µm) and layer distance (dZ, from 2.2 to 4.6 µm). All the printing experiments were performed at a fixed writing speed of 1000 mm.s-1 (general process flow is shown in SD1).

After 2PP structuring, a similar development protocol was applied as previously reported for PCL-based resins [38], the sample holder was submerged in tetrahydrofuran (THF) to dissolve remaining uncrosslinked material. Two additional THF washing steps of the 2PP printed structures were carried out before a final storing and sterilization in 1-propanol.

2.2. Spheroids formation, culture condition and differentiation assay

Prior to cell seeding, the microscaffolds were sterilized in 1-propanol and deposited manually in homemade agarose mold containing multiple 2 µL wells (process shown Fig. 2). The solvent was left to dry under laminar flow and molds were incubated at least 3 days in medium (EGM-2, composition presented thereafter), with medium changed daily. Immortalized human adipose-derived mesenchymal stem cells (hASC/hTERT) (Evercyte, Austria) were expanded using EGM-2 BulletKit^{TM} medium (Lonza, Switzerland) supplemented with 10% (v/v) newborn calf serum (NBCS) (Gibco, New Zealand) and maintained at standard culturing conditions (37 °C, 5% CO_2, humidified atmosphere). 2 µL of hASCs suspension (containing 5000 cells, passages 6–7) were seeded manually into each well (containing one BB each or free of BB for normal spheroid group (SPH)) and let to form spheroids for 2 days.

The seeding efficiency was calculated as followed, with the "DNA day 0" corresponding to the initial amount of DNA present in 5000 hASCs (n=3).

$$\text{Seeding efficiency (in \%)} = \frac{DNA\ day\ 2\ per\ spheroid}{DNA\ day\ 0} * 100$$

2-day post-seeding, the medium was replaced by normal medium, except otherwise stated (composed of high glucose Dulbecco's modified Eagle medium [HG-DMEM; Gibco, United Kingdom] supplemented with 10% NBCS and 1% penicillin-streptomycin). The medium was changed two to three times a week for 28 days.

For the differentiation assay, similar work-flow was followed, except that EGM-2 was replaced by either chondrogenic (CM) or osteogenic medium (OM); HG-DMEM serving as control medium. CM consisted of HG-DMEM supplemented with 1% (v/v) Insulin-Transferrin-Selenium Supplement (Gibco, UK), 1% (v/v) of P/S, 1% (v/v) 1 M HEPES buffer (Mediatech, VA, USA), 0.1 mg/mL sodium pyruvate, 50 µg/mL L-proline, 50 µg/mL ascorbic acid 2-phosphate, 100 nM dexamethasone, 10 ng/mL of human transforming growth factor β3(Peprotech, NY, USA) and human bone morphogenic protein 6 (R&D, MN, USA). OM was composed of HG-DMEM supplemented with 10% (v/v) NBCS, 4 mM L-glutamine, 1% (v/v) P/S, 10 nM dexamethasone, 150 µM ascorbic acid 2-phosphate, 10 mM β-glycerophosphate and 10 nM 1,25-Vitamin D3.

The fusiogenic ability of multiple SPH and BB was assessed on 2-day old specimen (involving either doublets or 20 units), by incubating them on a U-bottom low-binding 96 well plate (Lipidure-Coat Low adhesion plate, Amsbio, USA). Samples were kept in control medium as previously described. Images were taken at regular time-points during the experiment and processed using ImageJ to analyze the area, the roundness and the intersphere angle of the fusing units, as done by others [39]. For all the *in vitro* experiments, the media were changed three times a week for a period of 14 up to 28 days, depending on the experiment.

2.3. Macroscopic and microscopic characterizations

Images of SPHs and BBs were taken using a LSM 700 confocal microscope (Zeiss, Germany). Shape descriptor from ImageJ was then employed to determine the diameter (maximal Feret diameter), the roundness of the spheroid structures (with perfect sphere = 1.0), the area and the intersphere angle (n>10). Scanning electron microscopy (SEM) analysis was performed after fixation in buffered paraformaldehyde at 4%, followed by gradual dehydration in ethanol and by immersion in hexamethyldisilazane (Sigma-Aldrich). After drying, the samples were sputter-coated with Au and investigated by SEM (Philips XL Series 30). Sectioning of spheroids and BB-loaded spheroids was performed using focused ion beam (FEI DualBeam FIB Quanta 3D). This required the samples to be sputter coated with a 4 nm thick Au Pd-layer to provide conductivity. Before the actual sectioning, the position of interest on the sample was protected by depositing a 2 and 3 µm thick Pt-layer. Sectioning was then done with decreasing ion beam intensities (from 30 kV, 30 nA through to 30 kV, 10 pA) in order to produce a smooth surface and to minimize damage of the microstructure. The samples were then imaged using SEM (FEI FEGSEM Quanta 250F).

2.4. Cytotoxicity assays (ISO 10993-5)

Extract cytotoxicity assay was performed by incubating 6 BBs in two different extraction vehicles, i.e. either 150 µL of normal medium or 25 µL of dimethyl sulfoxide (DMSO) at 37 °C, as recommended here [40]. Three times a week, the supernatants were removed and used to feed monolayer of fibroblast L-929 (seeded at 3000 cells/well in 96-well plate, from Sigma-Aldrich). The control group consisted of BB-free medium. To prevent any DMSO-associated cytotoxicity issue, a final dilution of DMSO to 0.1% was performed with normal medium before feeding the cells monolayer. Metabolic activity of the L-929 monolayer was assessed using PrestoBlue^{TM} Cell Viability Reagent (Invitrogen, Fisher Scientific, Vienna, Austria) from day 0 (which corresponded to one day post-seeding, just before starting the feeding test with supernatant) until confluence of the monolayer (day 21, n=6/condition). Fluorescence was chronologically recorded at 560/590 nm using a spectrophotometer (Synergy H1 BioTeK^{TM} plate reader, Bad Friedrichshall, Germany).

Direct cytotoxicity assay was conducted after formation of hASC spheroids inside BBs (control group consisted of normal spheroids, SPH) and cultivated in normal medium, as described before. At different time points, BBs or SPHs were removed, washed twice with PBS and incubated with 100 µL of CellTiter-Glo®3D (Promega, Walldorf, Germany) and an equal amount of normal medium (1:1) for 20 min under agitation at room temperature [41]. The samples were then left 5 min and luminescence was quantified using spectrophotometer (n =6/group/time point). In addition, viability of the cells was determined using a Live/Dead® assay (Invitrogen, thermofisher) using 0.2 µM calcein-AM (live stain) and 0.6 µM propidium iodide (dead stain) in serum-free medium for 60 min at 37 °C. The viability of cells was monitored on day 3 and on day 28, using a confocal laser scanning microscope LSM 800 (Zeiss, Germany). The quantification of the viability of the cells was assessed by removing the spheroids for culture medium at defined

time points (4, 12, 28 and 34 days), washing them with PBS and incubating them in a Trypsin-EDTA solution (BioReagent, Sigma-Aldrich) for 15 min at 37 °C. The samples were then vortexed to facilitate spheroids disaggregation, and viable cells were visualized using an optical microscope after Trypan Blue staining (n=3 for each group and time point).

2.5. Biochemical assays

DNA quantification was done after sample digestion, as followed. At different time points (from day 0 corresponding to the cell suspension with 5000 hASCs up to day 32), samples were washed with PBS and digested with 125 µg/mL papain in 0.1 M sodium acetate, 10 mM L-cysteine-HCl, 50 mM EDTA (all from Sigma-Aldrich) adjusted pH 6.0 and incubated at 55 °C under constant shaking for 18 h. DNA content of each sample was quantified using the Quant-iT PicoGreen assay (Thermofisher, USA) (n = 3 for each group).

The content of sulfated glycosaminoglycans (sGAG) of samples cultivated in CM compared to normal medium was quantified using the dimethylmethylene blue dye-binding assay (DMMB, Blyscan, Biocolor Ltd., United Kingdom), with a chondroitin sulphate standard, and the values were normalized against DNA (n=5 and 6).

The total amount of extracellular matrix (ECM) deposited within the spheroids was analyzed by first, dissolving the proteins from the samples using a 0,5% Triton™ X-100 (Sigma-Aldrich) solution in dH_2O. To facilitate the disaggregation, the samples were mixed with a dispersing instrument (Ultra-turrax, IKA, Staufen im Briesgau, Germany) for 2 min. The resulting solutions were subjected to protein assay quantification following the recommendation of the supplier (CBQCA Protein Quantitation Kit, Thermofisher) (n=5).

The content of calcium deposition of samples cultivated in OM compared to normal medium was quantified using a colorimetric calcium quantification kit (Calcium Assay Kit ab102505, abcam, Cambridge, United Kingdom) according to manufacturer's protocol. Briefly, SPH and BB were collected (on day 28), washed in PBS, and subsequently resuspended in 500 µL Calcium Assay Buffer (supplied in the mentioned kit). Samples were homogenized on ice using the dispersing instrument (Ultra-turrax, IKA) for 2 min. Samples were spun at 10.000 g for 5 min at 4°C and the supernatants were transferred into new tubes for quantification as recommended by the supplier (n=3, per group).

2.6. Histology

After 1 and 28 days of cultivation, SPHs and BBs were washed in PBS and fixed overnight in Roti®Histofix 4% (Carl Roth, Germany) at 4°C. Samples were embedded in paraffin blocks and processed at the Histopathology Department (Vienna BioCenter Core Facilities GmbH, Austria) for Hematoxylin-Eosin (H&E), Von Kossa and Alcian Blue staining and for proliferative marker Ki-67. Images were acquired using a confocal microscope (LSM700, Zeiss, Germany). Zonal repartition of the dividing cells was evaluated by manually counting the number of Ki-67+ cells present at the periphery (representing the superficial 30% area) and at the center (representing the remaining 70% inner area) of the cut sections.

2.7. Statistical analyses

Statistical analysis of data was performed using Prism software (GraphPad Software, La Jolla, CA, USA). We assumed normal distribution of data. A student t-test was applied to detect significant differences between the two experimental groups (with $p < 0.05$). Data presented are means ± standard deviation (SD) unless stated otherwise.

3. Results

A prerequisite for the third TERM strategy, is first to be able to produce microscaffolds which can host single multicellular spheroids in their core. In order to define an optimal 2PP processing window for the material (i.e. a PCL-based photosensitive resin), a first printability test was undertaken varying the laser power (using fixed values of hatch and dZ) on cubic structures (Fig. 1a). For all those printing tests, the laser writing speed was kept constant at 1000 $mm.s^{-1}$. A good structure quality was observed when cubes were printed using laser power between 40 and 100 mW. Below and above this processing window, the material either not fully polymerized, or burned. This is visible on the microscopic images by either a cube of reduced size (e.g. when 20 mW laser power was used) or by darker spots (appearing on top of the cubes when laser power at 120 mW upwards was used). From this preliminary test, we further fine-tuned the printability window, by selecting laser powers of 35 up to 85 mW, varying hatch and dZ values. This test was conducted on BB structures (CAD design is shown in Fig. 1b), with an overall diameter of 300 µm and a strut diameter of 35 µm. Printing BBs with low laser powers (i.e. 35 mW and 45 mW) resulted in numerous collapsed or malformed structures, independently of the hatch or dZ values selection (Fig. 1c and SD1). The quality of the structured BB improved by using higher laser powers. At 55 mW, dZ below 3.8 µm and hatch below 1.7 µm allowed to print BBs with already better quality. Structures printed at 65 mW showed a good shape fidelity with hatch up to 2.1 µm and dZ up to 4.2 µm (SD2 and Supplementary Table 1).

Similar results were obtained for structures printed at 75 mW and 85 mW. The main difference is that by using a laser power of 85 mW, we noticed that the window of printability was further increased, and BBs with appropriate architecture were obtained when the distance between the printed layer dZ was up to 4.2 µm and the line distance (hatch) up to 2.5 µm. SEM images corroborated this observation, as BB structures with good match to the CAD design were achieved when using dZ and hatch values of 3.8 and 1.7 µm respectively (Fig. 1d). When appropriate 2PP parameters are selected, the printed layers and lines in the struts are hardly visible. An example of a printing process for a BB is shown in Video 1. Sub-optimal dZ or hatch values resulted in fragile structures with visible printing patterns and thicker struts (Fig. 1d, the optimal range of printability is summarized in Supplementary Table 1). A laser power of 85 mW, dZ and hatch of 3.8 µm and 1.7 µm respectively were then selected for the production of BB microscaffolds further used in this study. SEM image analysis revealed that the BBs have a diameter of 300.4 +/-5.7 µm and struts of 35.4 +/-4.0 µm, which are close to the initial dimensions in the 3D CAD design (Fig. 1d).

V-bottom shaped low-binding agarose molds (Fig. 2a) allowed to create single hASC spheroids after 24 h of cell seeding (Fig. 2b and c). 5000 hASCs were seeded per well, as this density allowed to produce spheroids with a diameter of approximately 300-350 µm, which corresponds to the dimension of the BB structures (seeding optimization is shown SD3). The presence of BBs did not hamper the spheroid formation, as the cells agglomerated inside the porous microscaffolds, similarly to normal spheroids (Fig. 2c and Videos 2 and 3 for bright field and fluorescent confocal microscopy where GFP-labeled hASCs and BB microscaffolds appeared green and red respectively). SEM analysis revealed that one day after seeding, cells started to flatten, with a few round-shaped cells still present on the surface of the spheroid structure. Typical cell spreading patterns and filopodia were detected when using higher

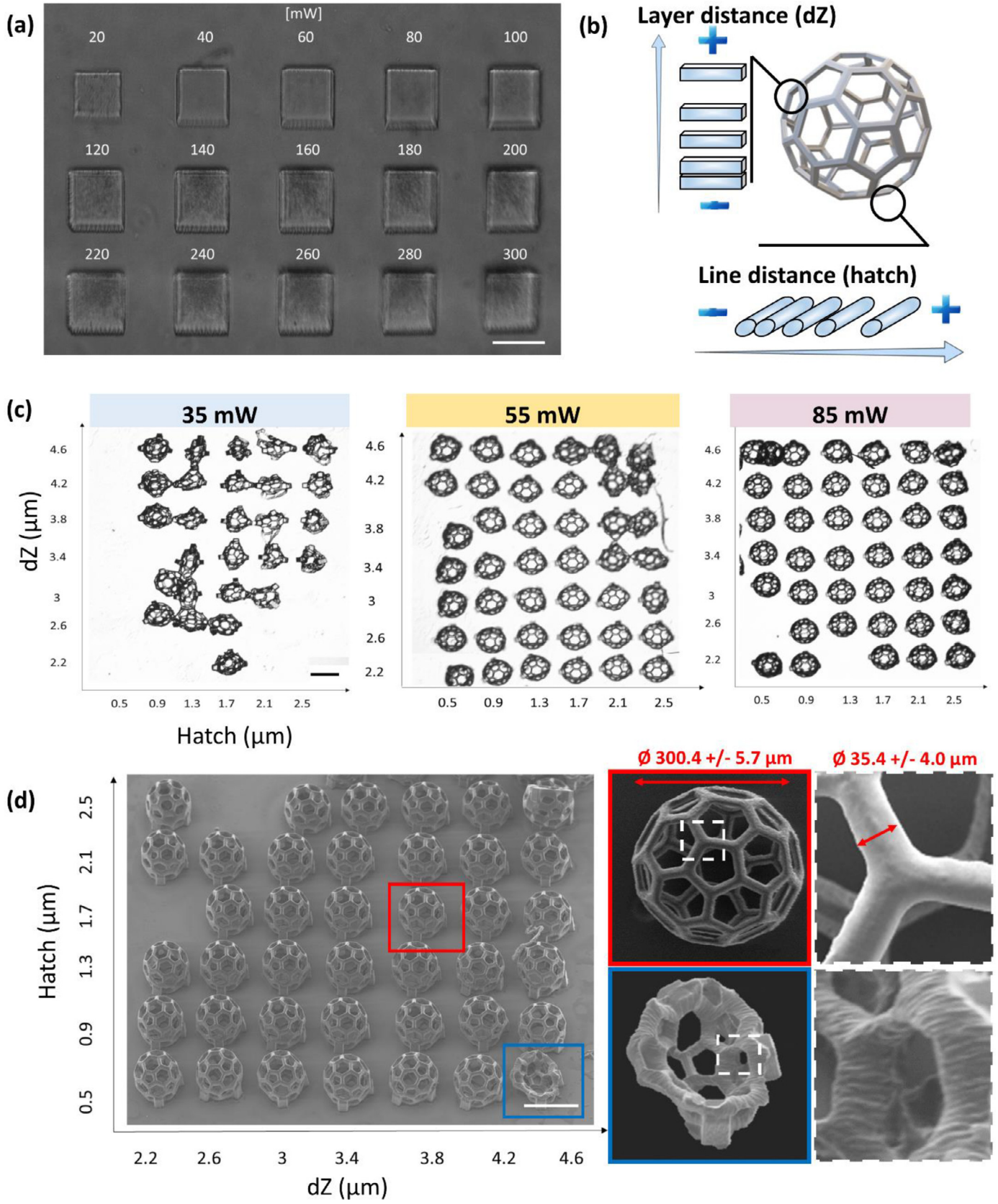

Fig. 1. Optimization of 2PP printing of PCL-based Degrad INX buckyballs.
Microscopic image of the printability test performed on cubes (100 × 100 × 100 µm³) with increasing laser power from 20 to 300 mW (fixed hatch and dZ values of 0.5 and 2.5 µm respectively, scale bar represents 100 µm), (**a**). Schematic representation of the line distance (hatch) and the layer distance (dZ) parameters for 2PP printing of BB (**b**). Arrays of BBs printed using increasing laser power (35, 55 and 85 mW), dZ and hatch values **(c).** SEM image of an array of BBs printed at 85 mW with varying hatch and dZ values, with inlets illustrating examples of BB printed with appropriate set-up and BB with suboptimal dZ **(d).** Scale bars in c and d represent 300 µm.

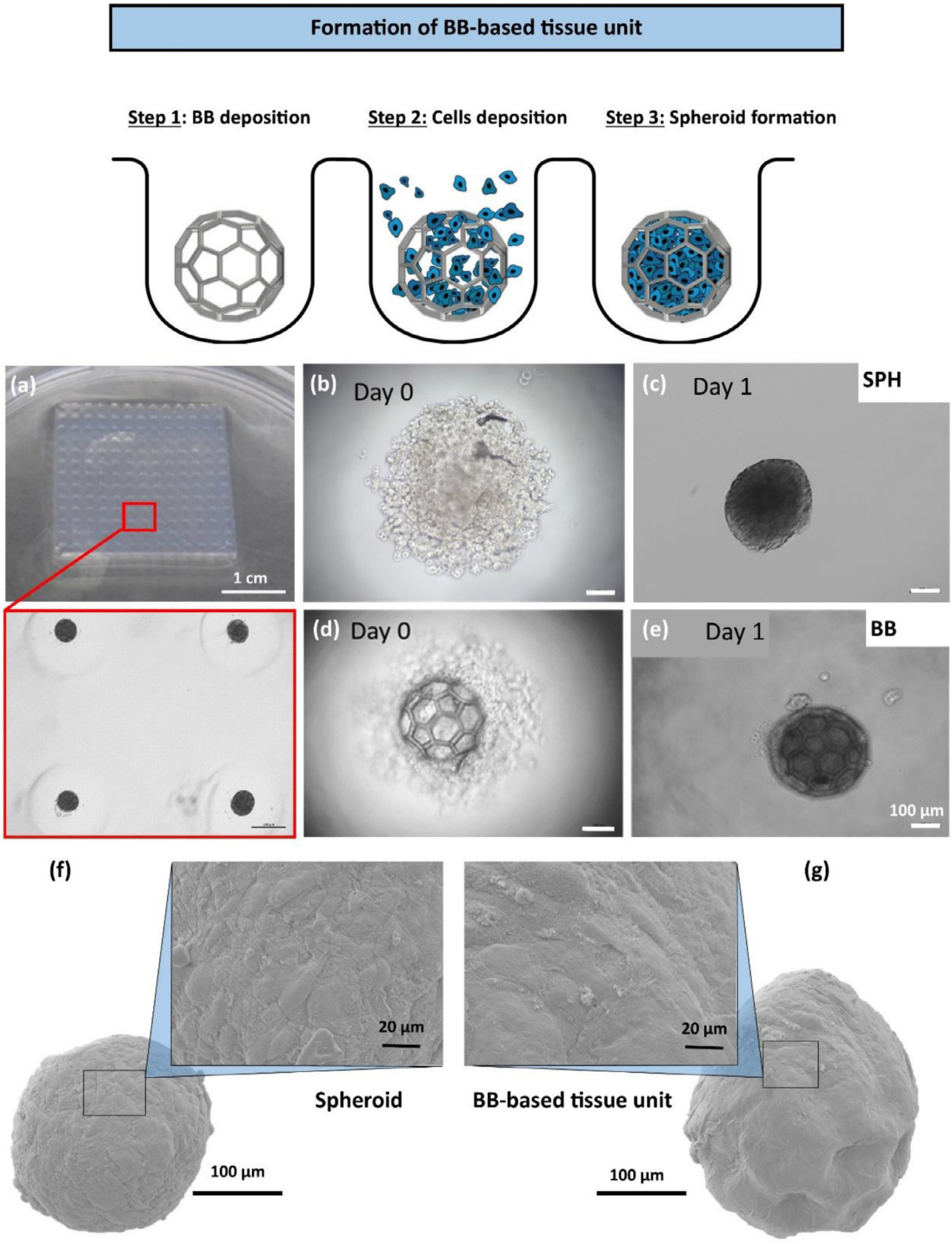

Fig. 2. Formation of buckyball-based tissue units and spheroids.
A custom-made agarose multi-well mold was used to create BB-based tissue units **(a).** 5000 hASCs were deposited in a 2 µL well (day 0, **b**) and agglomerated within 1 day into a single spheroid, SPH **(c).** To create BB-based tissue units, BBs are first manually deposited into each well followed by 5000 hASCs and left for 1 day for the cells to agglomerate together **(c).** SEM illustration of 1-day-old spheroid and BB (**d** and **e** respectively).

magnifications. Spheroids that formed inside BBs exhibited similar features as previously described. The cells fully invaded the porous core of the BB-structure, and only evidence of the struts was detectable by SEM (Fig. 2d and e).

Cytotoxicity studies were conducted according to the guidelines ISO10993-5. The extract test was assessed using exaggerated conditions. First, by using a higher amount of BBs / number of cells than usually required to form spheroids, and second, by using medium but also DMSO as the extract vehicle, as described in Fig. 3a [40]. The extract assay proved that the BB made of the photosensitive PCL-based resin did not have an impact on the L-929 fibroblasts monolayer, as their growth kinetics, recorded during the 21 days of the experiment, were not diminished in the BB-group compared to the control group (Fig. 3b). This was proven independently of the nature of the extract vehicle. Further, no difference in terms of cells spreading was noticed between the different experimental groups over the course of the test (as shown for day 7, SD4).

Additionally, a direct cytotoxicity assay was performed on spheroids formed without (control group, called SPH) or with supportive BB structures (called BB, Fig. 3c) incubated in normal

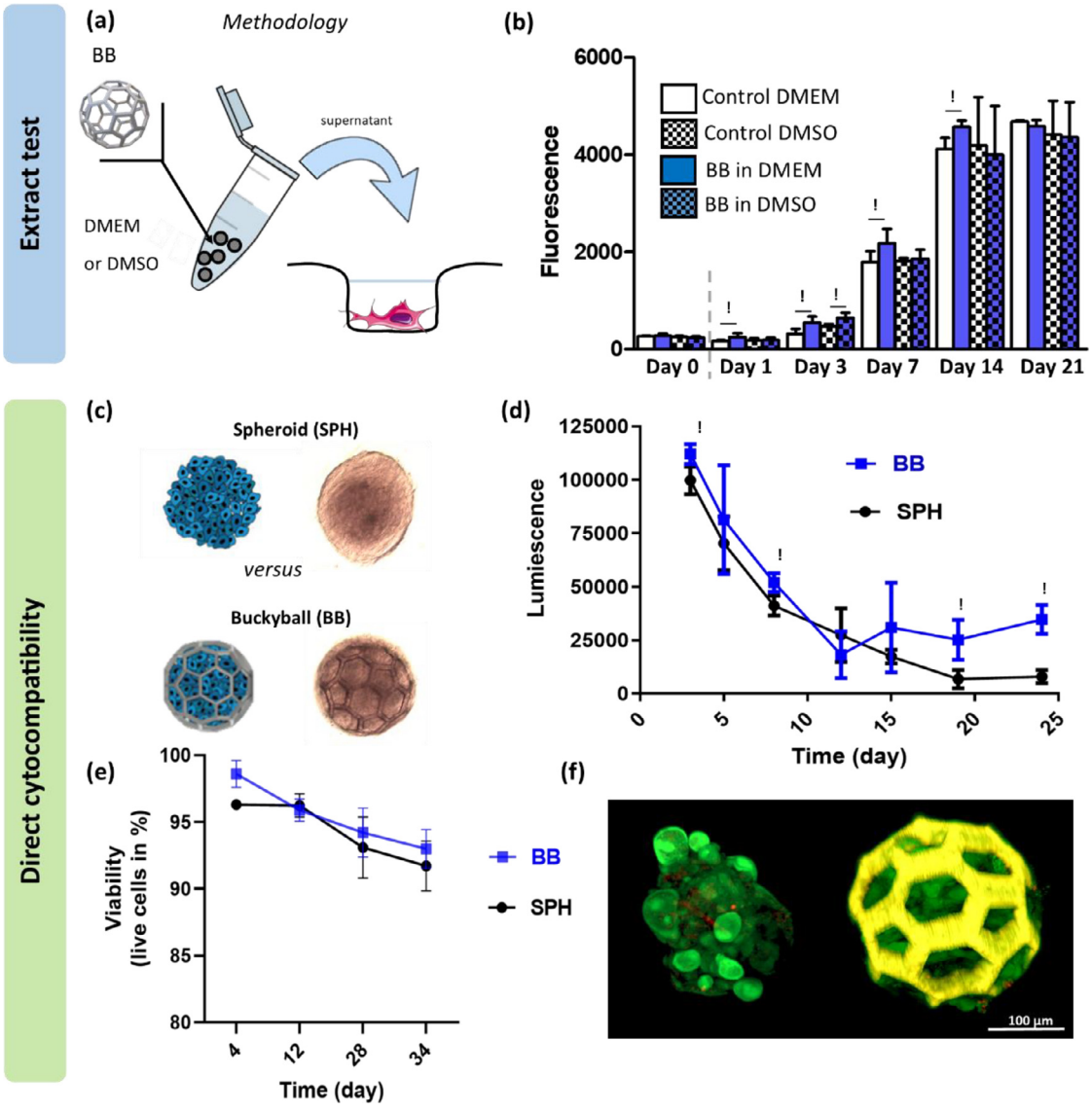

Fig. 3. ISO-10933 cytocompatibility tests of the photosensitive PCL-based Degrad INX©resin.
Extract cytotoxicity test was performed by incubating BBs in either control medium or DMSO, of which the supernatant was then used as feeding medium for L-929 fibroblasts monolayer (dilution 0.1 % in the case of DMSO), **a**. Cell-Titer Blue was conducted on the cell monolayer at different time points and the resulting fluorescence intensity at 560 nm was recorded (n=6). BB-incubated medium was compared to BB-free medium, consisting of control medium and DMSO at 0.1 % **(b).** Direct cytotoxicity assessment of hASC spheroids cultured within BBs (called BB) versus normal spheroids (called SPH, **c).** Cell-Titer Glo test was conducted to evaluate the metabolic activity (quantification of ATP by luminescence) at different time points (n=6, **d).** Cell viability in SPH versus BB was evaluated during 34 days of culture using Trypan Blue vital dye on re-suspended cells and was further visualized at day 28 using Live/Dead staining **(e** and **f)** ! denotes significance between BB and SPH (**b** and **d**).

medium (HG-DMEM with 10% NBCS). The ATP quantification revealed that the metabolic activity of SPH continuously decreased from day 1 to day 18 and plateaued until the end of the experiment (Fig. 3d). A similar trend was observed for the BB group, even though the ATP amount already reached a steady-state at day 15 and, consequently maintained values slightly, but significantly, higher than normal spheroids (Fig. 3d). To decipher if this drop of metabolic activity was due to an increased cell death, a viability study was conducted using Trypan Blue quantification assay and Live/Dead staining at different time points. As shown in Fig. 3e, the viability for both groups is suitable and remains above 90% over 34 days of experiment (with no statistical difference between SPH and BB). This result corroborated the Live/Dead staining performed at day 3 (SD5a) and day 28 (Fig. 3f). Both tests give the confirmation that the loss of ATP activity described previously is not due to an increased cell death.

Our next experiment demonstrated that not only the metabolic activity of SPH chronologically decreased but also their maximum Feret diameters (also called caliper diameter, Fig. 4a).

5000 agglomerated hASCs-formed spheroids with a diameter of approximately 400 µm, which then diminished down to 300 µm within 11 days, and to a final diameter of 225 µm after 28 days (Fig. 4a). BB-based tissue units started with a similar diameter than SPH but did not undergo such drastic size reduction. Their diameters stabilized after 11 days to 320-335 µm until the end of the experiment, which is slightly larger than the initially printed BB (Ø 300 µm). This first experiment was conducted in growth factor (GF)-free medium (HG-DMEM with 10% serum), but similar trends were noted when cells were cultivated in (GF)-enriched medium

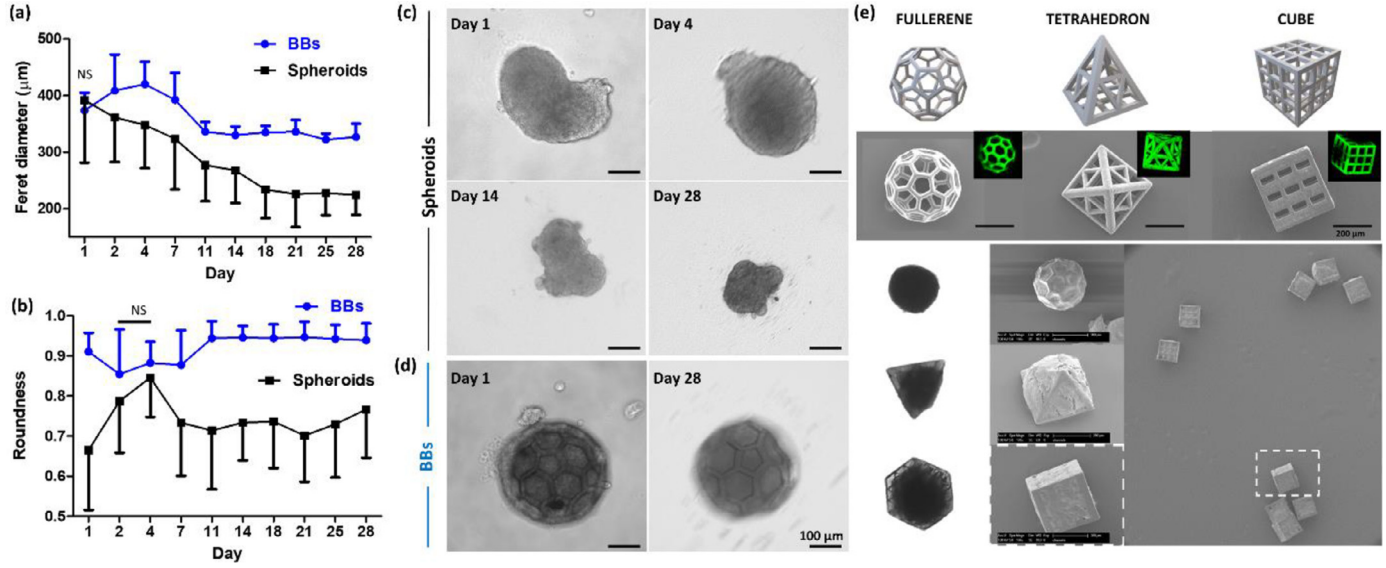

Fig. 4. Impact of the BB microscaffolds on the evolution of the spheroids' shape.
Evolution of the spheroids´diameter and roundness (**a** and **b**) and microscopic illustration of the SPH and the BB over time (**c** and **d**). Significative inter-group differences were reached for all of the time points, except where NS (non-significance) is noted. Cellular spheroids can be formed and confined themselves to the shape of the encaging structures (i.e. fullerene, tetrahedron and cube-shaped microscaffolds). Confocal, optical and SEM images of hASC-seeded microscaffolds after 4 weeks of cultivation (**e**).

(i.e. EGM-2 containing a cocktail of FGF, VEGF, IGF and EGF) (SD6), even though the difference after 28 days between the 2 groups was lower than in GF-free medium ($\Delta_{\text{BB-SPH in EGM2}}$ = 22% *versus* $\Delta_{\text{BB-SPH in DMEM}}$ 46% respectively).

The presence of the BB structures permitted to limit the volume reduction of the spheroids and also helped to maintain a better roundness. Roundness values comprised between 0.85 and 0.95 (where 1.0 equals a perfect sphere) for the BB group, and only between 0.65 and 0.85 for SPH (Fig. 4b). Macroscopic images confirmed such discrepancies. Under non-adhering growth conditions, hASCs agglomerated and formed SPH structures with a high deviation in terms of size and shape, and further showed a continuous decrease of diameter over time (Fig. 4c and d).

To emphasize on the potential of 2PP to fabricate intricate 3D structures, not only spheroid buckyballs with the fullerene shape can be produced but many other designs (such as tetrahedrons and cubes, Fig. 4e). It is interesting to note that cells formed compact agglomerates within microscaffolds of various shapes and confined themselves to their volume.

In the absence of BB structures, we observed that numerous cells were continuously released from the main spheroid bodies to the surrounding medium explaining the shape and size discrepancies previously described between SPH and BB groups (SD7a-d). The decrease in size and metabolic activity is the direct consequence of the reduced cell population. Indeed, there is a decrease of the amount of DNA per spheroid for both groups, but the mere presence of BB allowed to maintain a significantly higher cell number compared to normal spheroids SPH, from day 15 to day 32 (Fig. 5a). For both groups, a similar seeding efficiency of 78% was obtained, when comparing the amount of DNA corresponding to the cell suspension of 5000 hASCs deposited day 0 in each well, to the DNA value of 3-day-old SPH and BB. This means that 22% of the cells where not integrated in the forming spheroid and remained in the supernatant, independently of the absence or presence of microscaffolds.

BBs did not only have an impact on the cells' ability to proliferate, but also on the ECM secretion and spheroid compaction. The ECM quantification assay revealed that the trend for both groups in terms of protein secretion is similar, with a low amount of protein secreted over the first 10 days, which then significantly increases at later time point (i.e. day 24, Fig. 5b). It is interesting to note that the amount of protein secreted per sample for SPH compared to BB at day 24 is not significantly different when looking at the means, but there is a strong discrepancy in the standard deviations. Growing spheroids inside BB stimulated the ECM deposition in a more reproducible way than when no BB are present (SD are 5 and 30 µg/BB and µg/SPH respectively, Fig. 5b). As the amount of DNA per sample is approximately 5 times higher in BB *versus* SPH for such later time points (Fig. 5a), it is clear that a normalization of the amount of protein secreted per DNA (or per cell), will show significant higher values for SPH than for BB group. This heterogeneity in terms of ECM deposition for SPH group corroborates the trends observed when analyzing the size and roundness, as presented previous (Fig. 4).

The differences in terms of cellular density and ECM deposition are also apparent when looking at the spheroids' cross-sections processed for histology staining. H&E demonstrated that cells were homogeneously distributed throughout the SPH (Fig. 5c). In contrast, a lower packing density characterized with numerous intercellular cavities was seen already after only 1 day of BB spheroid formation, which remained throughout the duration of the experiment (Fig. 5d). Samples cut and observed using FIB-SEM corroborated such results, and revealed that the core of normal spheroids was dense with only a few small cavities. The tissue density was reduced for spheroids grown inside the BBs, with more and larger cavities.

Ki-67 is a nuclear protein, present in all phases of the cell cycle except G0, and is thus a marker for dividing cells. Immunostaining of the Ki-67 proliferative marker revealed that the number of cells undergoing division decreased significantly overtime, for both SPH and BB groups (Fig. 5e). For both groups and for both time points, the proliferative cells were mostly located at the peripheral rim of the structures and significantly less Ki-67+ cells were detected in the central part. Even though the differences were not significant, the zonal repartition at day 1 was slightly different between SPH and BB, where more dividing cells were seen in the center of the spheroids cultured within microscaffolds. This difference in terms of spatial repartition became significant at day 28, as no Ki-67+ cells could be detected in the center of normal spheroids SPH, compared to 9.3% for the BB group (Fig. 5f and g).

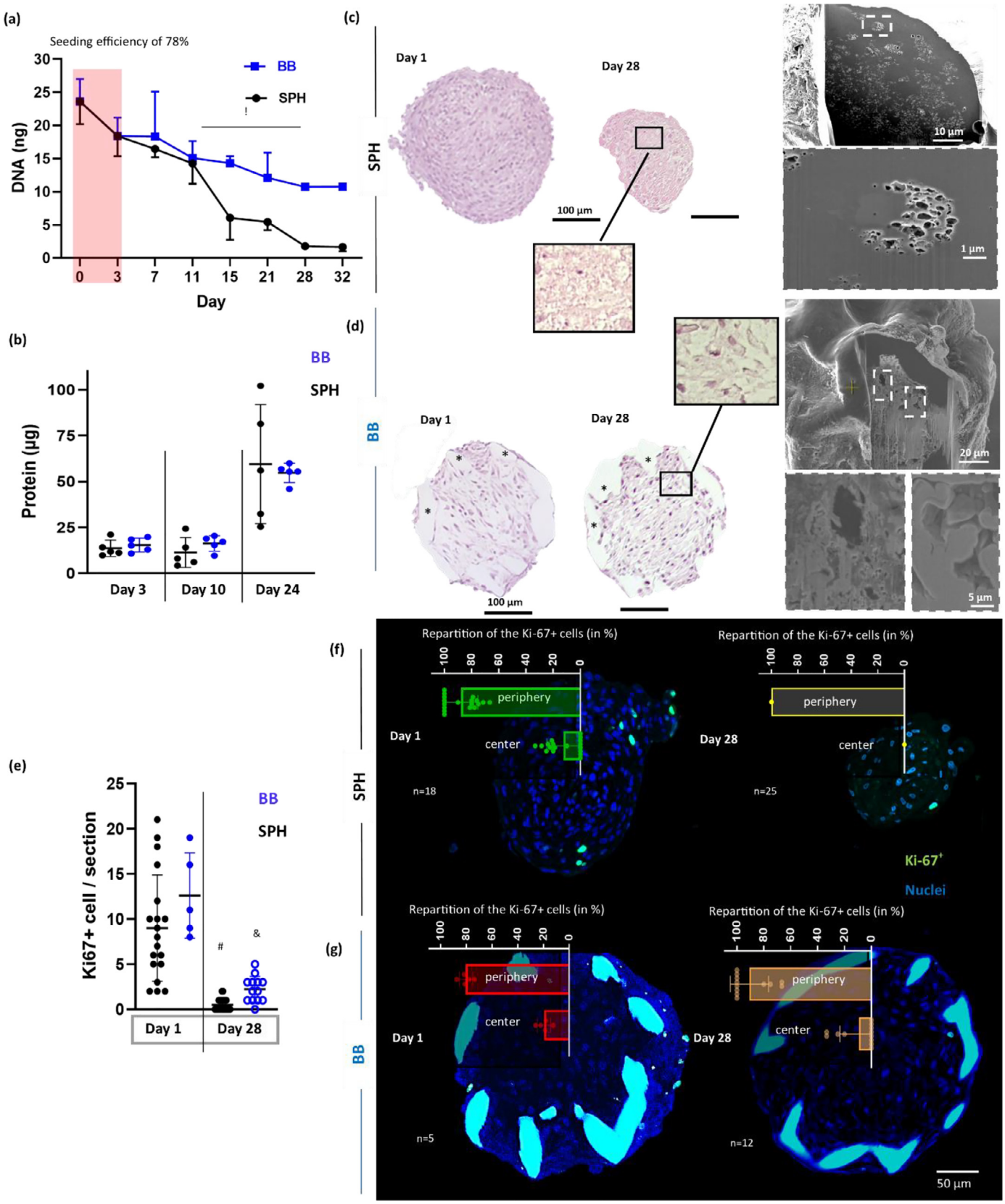

Fig. 5. Influence of the BB microscaffolds on the spheroid development.
Chronological evolution of DNA and protein content in SPH and BB (**a** and **b** respectively), ! denotes significance between SPH and BB groups. Histological staining (hematoxylin eosin) at day 1 and day 28 and FIB SEM cross-section after 28 days of SPH (**c**) and BB (**d**). The stars denote the strut of the generated BBs (**d**).
Comparison of Ki67+ proliferative cells for both groups from histological sections (**e,** statistically significant difference was only found between day 1 and day 28 for SPH # and for BB &). Histological immunostaining of green Ki-67+ cells counterstained with DAPI (blue nuclei) at day 1 and 28, for SPH versus BB (**f** and **g** respectively) with quantification of the zonal repartition of the Ki-67+ cells (center versus periphery, expressed in percentage).

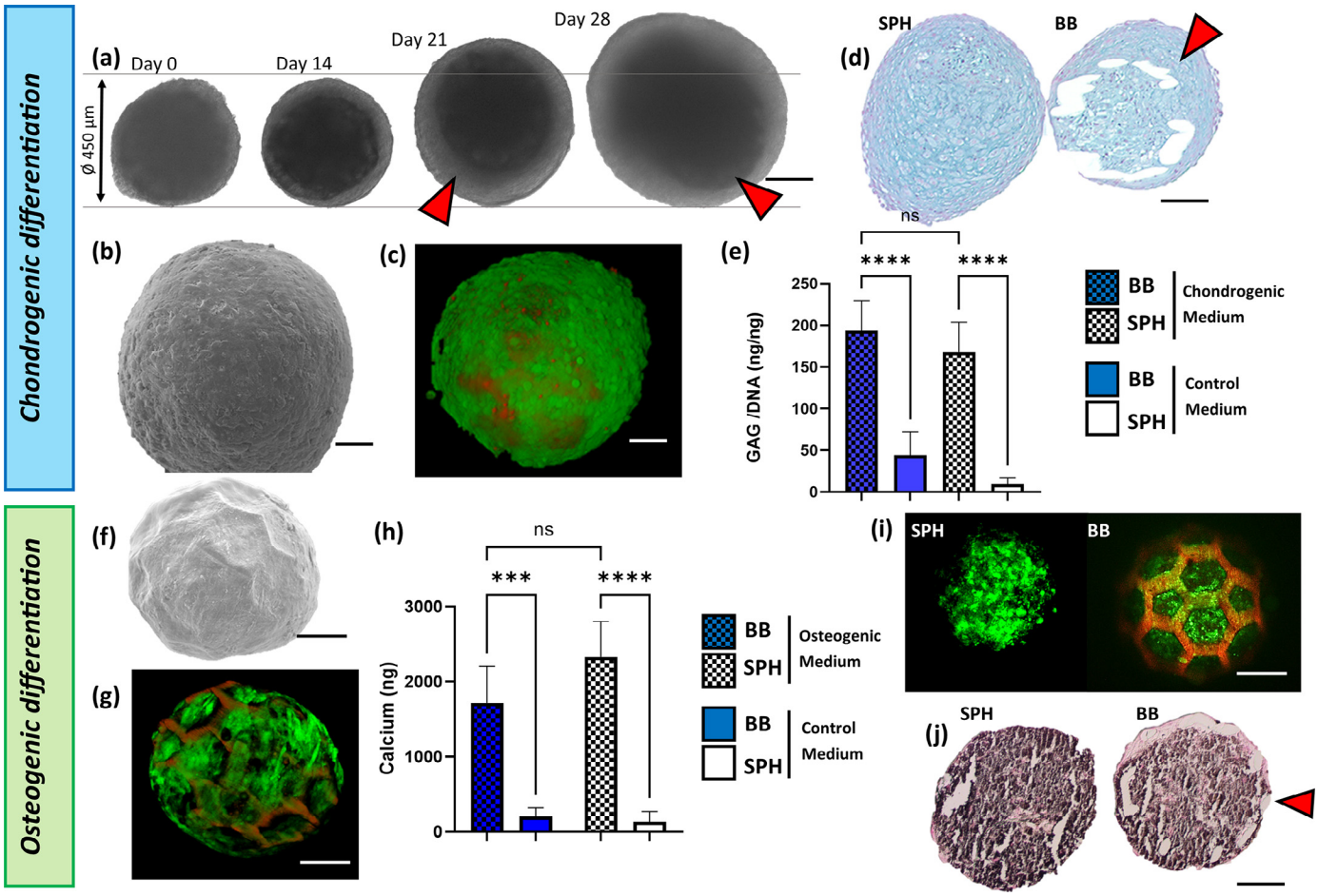

Fig. 6. Culturing hASC spheroids within microscaffolds does not impede their differentiation potential.
Assessment of BB chondrogenesis: Microscopic illustrations of BB-based tissue units grown under chondrogenic medium (CM) condition (**a**). SEM and Live/Dead staining images of BB after 4 weeks of cultivation in CM (**b** and **c**). Alcian Blue histological staining and DMMB assay for sGAG deposition (**d** and **e**). Assessment of BB osteogenesis: SEM and Live/Dead staining images of BB after 4 weeks of cultivation in OM (**f** and **g**). Successful mineral deposition was proven by calcium quantification (**h**), calcein green fluorescent staining (**i**) and by Von Kossa histological staining (**j**). Scale bars represent 100 µm and the microscaffoldś structure is denoted by the red arrows. *** and **** denote significance with P values <0,001 and <0,0001 respectively.

To assess if this significant difference might have negative outcome on the cell behavior, we proceeded to a chondrogenic and osteogenic differentiation assay, comparing both SPH and BB using hASCs (Fig. 6). Under chondrogenic condition (CM), the size of both groups evolved similarly and reached after 4 weeks of cultivation an average Feret diameter of 550 µm and 563 µm (for SPH and BB respectively, SD8). This demonstrated that the presence of BB microscaffold does not hamper cells to grow through and over the polymeric structure (Fig. 6a and b). Nevertheless, we did observe for both groups at the end of the cultivation a high deviation of the sample's average Feret diameters, ranging from 450 µm up to 720 µm (SD8).

No significant cell death was observed at the end of the cultivation for both groups (Fig. 6c illustrates BB, data not shown for SPH group). Alcian Blue staining on histological sections and DMMB assay validated the important ECM deposition rich in sGAG with no difference between both groups (Fig. 6d and e). A similar experiment was undertaken by cultivating hASC-spheroids and BBs for 4 weeks in osteogenic medium (OM). In contrast to what was observed for CM, samples kept in OM decreased in size on a similar trend for both groups, even if being more pronounced for spheroids (decrease of 13% for BBs *versus* 30% for SPHs, SD8). Due to the limited cellular growth, the struts of the BB are still discernible on SEM images of 4-weeks old samples keep in OM (Fig. 6f). The viability remains satisfying until the end of the experiment, but the main difference comparing CM and OM, is that the cells at the surface of the SPH or BB exhibited a more round-shape phenotype for CM *versus* a more flattened one for OM (Fig. 6f and g).

Finally, the positive calcium mineralization for both SPH and BB groups cultured in OM was demonstrated by the calcium quantification assay, the positive fluorescent calcein green staining as well as the histological staining using Von Kossa, depicted in black (Fig. 6 h–j). No positive Von Kossa staining and limited sGAG deposition were observed for control samples maintained in HG-DMEM medium (SD9).

After having focused the first part of the experimental section on single units, we then assessed how multiple units behave once brought together. As our final objective is to engineer large tissues using BB as building blocks, a prerequisite is that the presence of the microscaffold does not impede their capacity to fuse.

Using 2 units (doublets) put close to each other, we could demonstrate that both SPH and BB groups could effectively coalesce within one day of contact (Fig. 7a, 48 h time-lapse movies of two merging SPHs and BBs are shown in Videos 4 and 5 respectively). The measurement of the intersphere angles confirmed that the kinetic of fusion was similar for both groups over the first three days of the experiment (Fig. 7b). Discrepancy appeared at later time points, with θ_{SPH} being superior of θ_{BB} (210° *versus* 170° respectively), which can simply be explained by the presence of

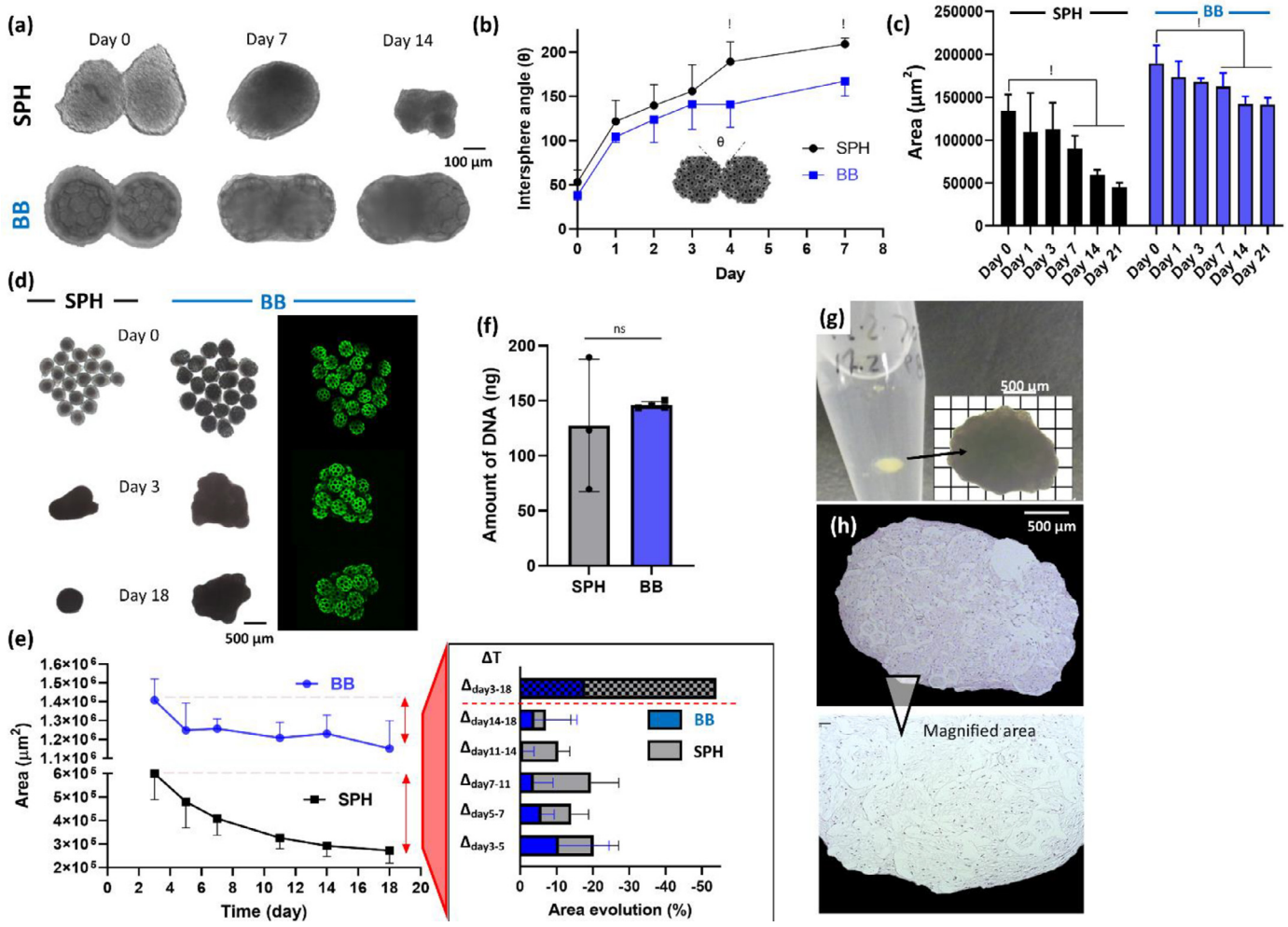

Fig. 7. Differences in spheroids' fusion due to the presence of BB microscaffolds.
Chronological evolution of one doublet of spheroids without and with the presence of BB, microscopically (**a**) and quantified by measuring the intersphere angle and the area evolution (**b** and **c**) (n=6). b- significance was only noted between SPH and BB at day 4 and 7 (denoted by !), c- inter-group differences were significant for all of the time points; ! denotes intra-group significance compared to day 0 only.
Larger self-assembled structures based on 20 SPHs or 20 BBs were formed and the size changes were visualized using optical and confocal microscopy over 18 days of culture (**d**). The diminution of the tissue area (in %) was calculated between each time point ($\Delta_{\text{day n - n+1}}$) for both groups (**e**, with the black square patterned bars representing the evolution over the entire duration time of culture) (n=4). The cellularity of the 18-day old structures was determined using DNA quantification (**f**) (n=3). Macroscopic observation and H&E staining image of a 28-day old and millimeter-size tissue assembly formed by the agglomeration of approximately 50 BBs **(g** and **h).**

the BB which physically restrains the merging of 2 units into a final "oblong-like shape" rather than a "sphere-like shape" as do doublets of SPHs. Nevertheless, significant morphological changes occurred as the SPHs underwent fusion, with the final size of this merged doublet being dramatically reduced compared to the initial units (Fig. 7a and c). Within 3 weeks of culture, the size reduction of 2 fused SPHs was close to 70% (Fig. 7c). As the BB acts as a "spheroid exoskeleton", two adjacent units may connect due to the high porosity, but cannot completely fuse. From this first study conducted on doublets, another fusiogenic investigation was performed using higher number of building blocks (20 per group). This study confirmed that multicellular assemblies can be formed starting from multiple SPHs but also from BBs, and that the presence of microscaffolds significantly reduces the tissue compaction occurring over maturation (Fig. 7d and e). At each time point, the decrease of the size of the engineered tissue construct resulting from the self-assembly of 20 units was significantly more pronounced for the SPH group than for the BB group. The size area decreased of 55% for SPH *versus* 17% for BB over 18 days of *in vitro* culture, which corroborated previous finding observed on single SPH and BB (Fig. 4a). NSF cells released from the tissues were also observed for the SPH and, to a less extend for the BB group (SD7e and f).

Even though the size of the self-assembled tissues demonstrates significative differences depending on the presence or absence of BB, the final number of cells within those tissues remains similar. Indeed, the DNA quantification performed at the end of the culture period (18 days) revealed similar amount for both groups, but with a more uniform distribution for BB than for SPH group (Fig. 7f). Finally, we showed that the size of the tissue assemblies can easily be up-scaled by increasing the number of BBs put together, reaching a millimeter-sized tissue that can hardly be attained using normal spheroid units (Fig. 7g and h). Once more, the cellular density within this macro-sized assembly is relatively low but its distribution is uniform throughout the section of the tissue. This highlights once more i- the advantage of using BB as building blocks for tissues with more control over the size and also over the cellularity than SPH, and, ii- the decreased tissue density in BB-based compared to SPH-based self-assemblies due to reduced compaction.

4. Discussion

Despite early successes observed when simply injecting spheroids into damaged tissues [11], the engineering of materials that could dictate the behavior of entrapped spheroids is an exciting strategy to potentiate the efficacy of spheroids. Recently, reports have suggested that merging the existing technologies will most likely bring unprecedented opportunities in the field of TERM [4,14,42]. The "third TERM strategy" enabling to build tissues through self-assembly of spheroids cultured inside microscaffolds is a good illustration of such direction. The possibility to actually create microscaffold-based tissue units has been presented in only few reports [36,37], but an investigation of the spheroids and cells behavior into such hybrid structure is urgently needed.

Forming spheroids within microscaffolds requires the latter to have an extremely high degree of porosity and large open pores with, consequently, very thin struts. In this study, the design of the microscaffolds was selected based on the chemical structure of a fullerene, referred to as buckyball (BB), since it is a spherical structure, highly porous with thin struts (i.e. of 35 µm), which was already shown to support spheroid formation within it [36,37]. Currently, producing such delicate structures is only possible using the 2PP technique. Other modern additive manufacturing techniques have been developed to produce scaffolds with sub-micron resolution (e.g. melt electrowriting [43]), which can then host spheroids. Such methods are nevertheless not suitable to produce suspended structures, which restricts their application and cannot be employed for the fabrication of multiple individualized BBs. In opposition, 2PP allows for direct laser writing within the volume of the resin. The resin, being highly viscous and solvent-free, further supports the realization of suspended microscaffolds.

Once optimal printing parameters were established, a high number of micro-sized structures could be produced in a reasonable time, without any post-processing deformation (see Supplementary Table 1). By using a writing speed of 1000 mm.s^{-1}, which is a current record for 2PP [44], the production of one single BB takes 10 sec. Using a single 2PP system, 6 days would be required to manufacture enough BBs to fill-up a defect volume of 1 cm^3 (using the hexagonal close packing model with packing fraction = 0.74, and a volume of 0.014 mm^3 per unit). Another aspect of the work-flow that deserves improvement is the extensive manual labor described to prepare the BB-based tissue units, which is currently not optimal for clinical translation. Tackling this bottleneck is possible by, for instance, using an automated system to distribute BBs into single wells of multiwell plates, followed by automatic liquid dispensing of the cell suspension. To conclude, we do not consider the entire work-flow being detrimental time-wise for a clinical usage, as the microscaffolds can easily be produced and sterilized in advance and be available off-the-shelf as soon as the patientś cells are available.

In summary, we have performed for the first time a systematic and comparative study between normal spheroids (SPH) and BB-based tissue units (BB). All experiments presented in this work were performed on spheroids of small-size diameter (300–350 µm) to decouple as much as possible the effects of the microscaffolds on the spheroids, from any nutrient- or oxygen-limiting effects [45–47].

We demonstrated that the presence of BB microscaffolds did not hamper some important features that made spheroids an attractive tool for TERM applications. First, we validated that a cell suspension can agglomerate to form a spheroid when cultured in low-binding condition, even in the presence of BB structures (Fig. 2). This can be explained by i- the design of the highly porous BB as previously emphasized, but also by ii- the hydrophobic nature of the chosen PCL-based material (±80°, as described here [38]), which does not support a rapid cellular attachment (shown SD10 on 2D films). Upon deposition of the cell suspension, cell-cell interaction will consequently become predominant, favoring the formation of the spheroid within the BB, rather than cells attaching onto its struts. hASC suspension formed a spheroid within BBs, with a seeding efficiency of 78%, similar to SPH. The presence of highly porous polymeric scaffolds does not impair the formation of the spheroids or their growth. To emphasize on the real effect of the BB microscaffolds on the spheroidś behavior, we have first selected a relatively lean medium (HG-DMEM with 10% serum but without any growth factor (GF) supplementation). As a result, it is clear that some of the reported features or at least their degree of intensity are medium-dependent (e.g. evolution of the diameter, shape, proliferation). Nonetheless, using a GF-enriched EGM-2 medium, we still observed the positive impact of BB microscaffolds on the spheroids ǵrowth (SD6).

It is recognized that scaffold-free aggregates used as building blocks allow to rapidly engineer larger tissues, with the advantage of a higher cell density compared to cell-seeded scaffolds. Nevertheless, a fundamental prerequisite for such biofabrication approach is that multiple spheroid bodies are able to coalesce together. Our set of data demonstrated that the fusiogenicity of hASC spheroids was not impaired by the presence BB microscaffolds (Fig. 7). In fact, multiple BBs self-assemble into a larger tissue when put into close contact in a kinetic similar to the one of SPHs only. The quality of the engineered tissue is in some aspects even favored by the BB, as the presence of a hard polymeric "exoskeletal" structure surrounding the cellular spheroid body prevented excessive compaction and condensation, which otherwise resulted in a final tissue of small and uncontrollable shape. The self-assembled tissues are indeed significantly more stable volume-wise when BB are used as building blocks. This characteristic will allow to accurately determine the number of spheroids required to fill up a defined volume of a certain tissue defect.

The spheroid-based tissue condensation is a natural phenomenon reported by many authors [2,19,21,22,48], but which can drastically restrict the clinical application of such bottom-up tissue engineering approach. Our study points out that this third tissue engineering strategy offers unprecedented opportunities in the future, but raises as well plenty of unanswered questions. For instance, condensation mechanisms are fundamental to tissue development but culturing spheroids within BB attenuates this phenomenon to a certain degree. Histological cross-sections revealed that there is an important difference in terms of cellular distribution between SPH and BB groups. Normal spheroids are characterized by a homogeneous and dense cell distribution throughout the volume of the structure. However, cells growing in the core of the BBs were more dispersed, less dense, had a polygonal shape and formed more intercellular cavities, as observed both histologically and on the FIB SEM cut sections (Fig. 5). The shape of the cells and the packing density appeared to be drastically impacted by the BB structures, but the ECM secretion (e.g. total protein, sGAG and mineral) were not significantly different. Similar features were described on large spheroids, and it was suggested that those resulted from an adaptive response of the cells present inside the spheroids to counter limited nutrient or oxygen diffusion, in an aim to prevent any detrimental effect on the cells [47]. Even though the viability study presented here did not reveal a higher degree of cell death in the BB group, further experiments are needed to specifically investigate the possible shortage of oxygen experienced by the cells in the center of the structure. One future avenue opened thanks to the high versatility of 2PP would be to adapt the shape or the size of the BBs (proof of concept shown Fig. 4e), which might then affect the occurrence of such cavities by controlling the degree of hypoxia.

Another interesting biological feature that was affected by the presence of the BB is that numerous non-spheroid forming (NSF)

cells were continuously released from normal spheroids. The expulsion of those loosely associated cells from the spheroids was responsible for a decrease of their cell number, and consequently a reduced diameter and roundness values. By growing the same spheroids inside porous BB structures, we were able to physically constrain the cells in a defined volume, and the resulting spheroids maintained a higher cellularity, a larger diameter and an improved roundness (close to 1, Fig. 4). Our data indicates that the BB act as a "cage" supporting the spheroid and maintaining cohesion between the cells as less NSF were observed in the BB group. E-cadherin plays an important role for the cell-cell adhesion and therefore for the preservation of spheroids. Stadler et al. proved that NSF cells that are expulsed from the main spheroid body have lost their E-cadherin expression [49]. The positive effect of BB structures on the cellular integrity of the spheroids may either stem from stimulated E-cadherin receptors or from a pure physical effect by retaining the cells and thereby forcing cell-cell interactions.

Our differentiation experiment on human adipose derived stem cells demonstrated that BB-based tissue units preserve the stemness potential of the spheroids, and that modules of bone and cartilage micro-tissues could be produced. This is also an important prerequisite as we aim to employ such tissue units as injectable building blocks for osteochondral tissue repair. If we are able to validate in future experiments that preventing cellular compaction does not affect the quality of the neo-formed tissue (such as an osteochondral tissue), then the utilization of microscaffolds such as BBs will greatly stimulate the development of spheroid-based therapies.

Even though we have not seen major differences in the fusion capability of multiple "young" spheroids, a recent report indicated that the ultrastructure of spheroid bodies impacts their fusion capability [50]. It was reported that an environment inside the spheroids that favors a rapid cell rearrangement, i.e. low ECM density, was correlated with a faster fusion kinetic. This aspect could then bring forward the necessity of using spheroid-loaded microscaffolds, which, as we indicated in this work, is responsible for a significant decrease of the spheroid packing density.

The actual bottleneck of using 2PP for TERM is the limited availability of biodegradable polymers processable using this technology, with only few reports on biodegradable polyesters to date [38,44]. As a photosensitive biomaterial, we tested a new commercially available biodegradable PCL-based resin (DDegrad INX). The high viscosity and high reactivity allow efficient processing even at extremely high scanning speeds of 1000 $mm.s^{-1}$ while providing a high strength to the printed structure. We have shown that not only biodegradable PCL-based resins, but also other biomaterials of interest can be processed using 2PP to build micro-size scaffolds, such as methacrylated poly-D,L-lactic acid (PDLLA) or methacrylated polycarbonate (PTMC, SD11).

Finally, this proposed strategy is truly convergent and versatile not only in the choice of biomaterials but also in the cellular composition, as many cell types can actually agglomerate into spheroids when cultivated under low-binding conditions. In this research, we used immortalized hASCs as a recent report has shown that this cell line maintains its stemness characteristic (even in high passage number), without the limiting irreproducibility seen using primary cells [51]. Other cell types can be integrated in the presented work-flow but this aspect would deserve further investigation, as the growth kinetics of spheroids are highly dependent on the cells and on the initial seeding density used to fabricate the spheroids [52].

Even though some questions remain unanswered, our work opens numerous perspectives and offers exciting venues for futuristic TERM strategies.

5. Conclusion

Some recent reports have raised awareness of a third approach in tissue engineering, which merges both scaffold-free and scaffold-based strategies by forming spheroids inside micro-size scaffolds; nonetheless little is known on how the cells behave inside such structures. In this original report, we first validate that, due to the high-resolution ability of 2PP, a high number of microscaffolds with a buckyball shape (BB) exhibiting fine architectural features can be produced. Such design was selected as it enables a cell suspension to agglomerate into spheroid within its core. Importantly, when spheroids of adipose derived stem cells are cultured within BBs, the spheroids maintain their differentiation potentials (i.e. chondrogenic and osteogenic). Another key aspect is that BB-based tissue units can be used as building blocks, which can fuse together and form macro-tissues through directed self-assembly, without external manipulations. The great advantage is that the volume of the resulting tissue is stable and easily controllable, as it is less prone to compaction. This singular property makes this approach highly suitable for the bottom-up utilization of hybrid spheroids as modular tissue units to be used in tissue engineering and regenerative medicine.

Declaration of Competing Interest

.

The authors declare the following financial interests/personal relationships which may be considered as potential competing interests:

A. Ovsianikov is a Co-Founder of UpNano GmbH, a recent spin-off of the TU Wien, which provided control software for the 2PP system. A. Arslan and S. Van Vlierberghe are in the founder team of BIO INX that commercializes Degrad INX.

Acknowledgment

This project has received funding from the European Research Council (ERC) under the European Union's Horizon 2020 research and innovation programme (Grant agreement No. 772464).We acknowledge the institute of Applied Synthetic Chemistry TU Wien, Dr. Blanquer S. from the Institute Charles Gerhardt Montpellier (France) for the synthesis of photo-sensitive PDLLA, Guo Z. from the Department of Biomaterials Science and Technology, Faculty of Science and Technology, Technical Medical Centre, University of Twente, Enschede (The Netherlands) for supplying the photosensitive PTMC, Riemenschneider F. for designing the tetrahedrons and cubic structures (TU Wien), Steiger W. for preparing the schematics in Fig. 2a (TU Wien) and Ferner T. for conducting the intersphere angle experiment (TU Wien). Van Vlierberghe S. would like to acknowledge the funding from Interreg 2Seas 3DMed.

Supplementary materials

Supplementary material associated with this article can be found, in the online version, at doi:10.1016/j.actbio.2022.03.010.

References

[1] J. Henkel, D.W. Hutmacher, Design and fabrication of scaffold-based tissue engineering, BioNanoMaterials 14 (3-4) (2013) 171–193.
[2] V. Mironov, R.P. Visconti, V. Kasyanov, G. Forgacs, C.J. Drake, R.R. Markwald, Organ printing: tissue spheroids as building blocks, Biomaterials 30 (12) (2009) 2164–2174.
[3] B.M. Holzapfel, J.C. Reichert, J.-T. Schantz, U. Gbureck, L. Rackwitz, U. Nöth, F. Jakob, M. Rudert, J. Groll, D.W. Hutmacher, How smart do biomaterials need to be? A translational science and clinical point of view, Adv. Drug. Deliv. Rev. 65 (4) (2013) 581–603.

[4] A. Ovsianikov, A. Khademhosseini, V. Mironov, The synergy of scaffold-based and scaffold-free tissue engineering strategies, Trends Biotechnol. 36 (4) (2018) 348–357.
[5] M.W. Laschke, M.D. Menger, Life is 3D: boosting spheroid function for tissue engineering, Trends Biotechnol. 35 (2) (2017) 133–144.
[6] A.R. Verissimo, K. Nakayama, Scaffold-free biofabrication, in: A. Ovsianikov, J. Yoo, V. Mironov (Eds.), 3D Printing and Biofabrication, Springer International Publishing, Cham, 2018, pp. 431–450.
[7] E. Fennema, N. Rivron, J. Rouwkema, C. van Blitterswijk, J. de Boer, Spheroid culture as a tool for creating 3D complex tissues, Trends Biotechnol. 31 (2) (2013) 108–115.
[8] K. Ishihara, K. Nakayama, S. Akieda, S. Matsuda, Y. Iwamoto, Simultaneous regeneration of full-thickness cartilage and subchondral bone defects in vivo using a three-dimensional scaffold-free autologous construct derived from high--density bone marrow-derived mesenchymal stem cells, J. Orthop. Surg. Res. 9 (1) (2014) 98.
[9] M.A. Gionet-Gonzales, J.K. Leach, Engineering principles for guiding spheroid function in the regeneration of bone, cartilage, and skin, Biomed. Mater. 13 (3) (2018) 034109.
[10] S. Uchida, K. Itaka, T. Nomoto, T. Endo, Y. Matsumoto, T. Ishii, K. Kataoka, An injectable spheroid system with genetic modification for cell transplantation therapy, Biomaterials 35 (8) (2014) 2499–2506.
[11] S.H. Bhang, S. Lee, J.Y. Shin, T.J. Lee, B.S. Kim, Transplantation of cord blood mesenchymal stem cells as spheroids enhances vascularization, Tissue Eng. Part A 18 (19-20) (2012) 2138–2147.
[12] H. Favreau, L. Pijnenburg, J. Seitlinger, F. Fioretti, L. Keller, D. Scipioni, H. Adriaensen, S. Kuchler-Bopp, M. Ehlinger, D. Mainard, P. Rosset, G. Hua, L. Gentile, N. Benkirane-Jessel, Osteochondral repair combining therapeutics implant with Mesenchymal stem cells spheroids, Nanomed. Nanotechnol. Biol. Med. (2020) 102253.
[13] Y. Xu, T. Shi, A. Xu, L. Zhang, 3D spheroid culture enhances survival and therapeutic capacities of MSCs injected into ischemic kidney, J. Cell. Mol. Med. 20 (7) (2016) 1203–1213.
[14] J.W. Nichol, A. Khademhosseini, Modular tissue engineering: engineering biological tissues from the bottom up, Soft Matter 5 (7) (2009) 1312–1319.
[15] J.I. Lee, M. Sato, H.W. Kim, J. Mochida, Transplantatation of scaffold-free spheroids composed of synovium-derived cells and chondrocytes for the treatment of cartilage defects of the knee, Eur. Cell Mater. 22 (2011) 275–290 discussion 290.
[16] A.C. Daly, M.D. Davidson, J.A. Burdick, 3D bioprinting of high cell-density heterogeneous tissue models through spheroid fusion within self-healing hydrogels, Nat. Commun. 12 (1) (2021) 753.
[17] V. Mironov, J. Zhang, C. Gentile, K. Brakke, T. Trusk, K. Jakab, G. Forgacs, V. Kasyanov, R.P. Visconti, R.R. Markwald, Designer 'blueprint' for vascular trees: morphology evolution of vascular tissue constructs, Virtual Phys. Prototyp. 4 (2) (2009) 63–74.
[18] A.M. Blakely, K.L. Manning, A. Tripathi, J.R. Morgan, Bio-pick, place, and perfuse: a new instrument for three-dimensional tissue engineering, Tissue Eng. Part C Methods 21 (7) (2015) 737–746.
[19] K. Jakab, A. Neagu, V. Mironov, R.R. Markwald, G. Forgacs, Engineering biological structures of prescribed shape using self-assembling multicellular systems, Proc. Natl. Acad. Sci. U.S.A. 101 (9) (2004) 2864–2869.
[20] C.M. Livoti, J.R. Morgan, Self-assembly and tissue fusion of toroid-shaped minimal building units, Tissue Eng. Part A 16 (6) (2010) 2051–2061.
[21] A.P. Rago, D.M. Dean, J.R. Morgan, Controlling cell position in complex heterotypic 3D microtissues by tissue fusion, Biotechnol. Bioeng. 102 (4) (2009) 1231–1241.
[22] E. Vrij, J. Rouwkema, V. LaPointe, C. van Blitterswijk, R. Truckenmüller, N. Rivron, Directed assembly and development of material-free tissues with complex architectures, Adv. Mater. 28 (21) (2016) 4032–4039.
[23] B. Ayan, D.N. Heo, Z. Zhang, M. Dey, A. Povilianskas, C. Drapaca, I.T. Ozbolat, Aspiration-assisted bioprinting for precise positioning of biologics, Sci. Adv. 6 (10) (2020) eaaw5111.
[24] N.I. Moldovan, N. Hibino, K. Nakayama, Principles of the Kenzan method for robotic cell spheroid-based three-dimensional bioprinting, Tissue Eng. Part B Rev. 23 (3) (2017) 237–244.
[25] D. Murata, K. Arai, K. Nakayama, Scaffold-free bio-3D printing using spheroids as "Bio-Inks" for tissue (Re-)construction and drug response tests, Adv. Healthc. Mater. (2020) e1901831.
[26] Y. Du, M. Ghodousi, E. Lo, M.K. Vidula, O. Emiroglu, A. Khademhosseini, Surface-directed assembly of cell-laden microgels, Biotechnol. Bioeng. 105 (3) (2010) 655–662.
[27] Y. Du, E. Lo, S. Ali, A. Khademhosseini, Directed assembly of cell-laden microgels for fabrication of 3D tissue constructs, Proc. Natl. Acad. Sci. 105 (28) (2008) 9522–9527.
[28] B. Zamanian, M. Masaeli, J.W. Nichol, M. Khabiry, M.J. Hancock, H. Bae, A. Khademhosseini, Interface-directed self-assembly of cell-laden microgels, Small 6 (8) (2010) 937–944.
[29] S. Xin, D. Chimene, J.E. Garza, A.K. Gaharwar, D.L. Alge, Clickable PEG hydrogel microspheres as building blocks for 3D bioprinting, Biomater. Sci. 7 (3) (2019) 1179–1187.
[30] J.G. Fernandez, A. Khademhosseini, Micro-masonry: construction of 3D structures by microscale self-assembly, Adv. Mater. 22 (23) (2010) 2538–2541.
[31] N.N. Kachouie, Y. Du, H. Bae, M. Khabiry, A.F. Ahari, B. Zamanian, J. Fukuda, A. Khademhosseini, Directed assembly of cell-laden hydrogels for engineering functional tissues, Organogenesis 6 (4) (2010) 234–244.
[32] A. Leferink, D. Schipper, E. Arts, E. Vrij, N. Rivron, M. Karperien, K. Mittmann, C. van Blitterswijk, L. Moroni, R. Truckenmüller, Engineered micro-objects as scaffolding elements in cellular building blocks for bottom-up tissue engineering approaches, Adv. Mater. 26 (16) (2014) 2592–2599.
[33] A.M. Leferink, M.P. Tibbe, E.G.B.M. Bossink, L.E. de Heus, H. van Vossen, A. van den Berg, L. Moroni, R.K. Truckenmüller, Shape-defined solid micro-objects from poly(d,l-lactic acid) as cell-supportive counterparts in bottom-up tissue engineering, Mater. Today Bio 4 (2019) 100025.
[34] T. Ren, W. Steiger, P. Chen, A. Ovsianikov, U. Demirci, Enhancing cell packing in buckyballs by acoustofluidic activation, Biofabrication 12 (2) (2020) 025033.
[35] J. Li, X. Li, T. Luo, R. Wang, C. Liu, S. Chen, D. Li, J. Yue, S.H. Cheng, D. Sun, Development of a magnetic microrobot for carrying and delivering targeted cells, Sci. Robot. 3 (19) (2018) eaat8829.
[36] K.R. Silva, R.A. Rezende, F.D.A.S. Pereira, P. Gruber, M.P. Stuart, A. Ovsianikov, K. Brakke, V. Kasyanov, J.V.L. da Silva, J.M. Granjeiro, L.S. Baptista, V. Mironov, Delivery of human adipose stem cells spheroids into lockyballs, PLoS One 11 (11) (2016) e0166073.
[37] P. Danilevicius, R.A. Rezende, F.D.A.S. Pereira, A. Selimis, V. Kasyanov, P.Y. Noritomi, J.V.L.d. Silva, M. Chatzinikolaidou, M. Farsari, V. Mironov, Burr-like, laser–made 3D microscaffolds for tissue spheroid encagement, Biointerphases 10 (2) (2015) 021011.
[38] A. Arslan, W. Steiger, P. Roose, H. Van den Bergen, P. Gruber, E. Zerobin, F. Gantner, O. Guillaume, A. Ovsianikov, S. Van Vlierberghe, P. Dubruel, Polymer architecture as key to unprecedented high-resolution 3D-printing performance: The case of biodegradable hexa-functional telechelic urethane-based poly-ε-caprolactone, Mater. Today (2020).
[39] A. Gryadunova, J. Kasamkattil, M.H.P. Gay, B. Dasen, K. Pelttari, V. Mironov, I. Martin, S. Schären, A. Barbero, O. Krupkova, A. Mehrkens, Nose to Spine: spheroids generated by human nasal chondrocytes for scaffold-free nucleus pulposus augmentation, Acta Biomater. 134 (2021) 240–251.
[40] ISO 10993: Biological evaluation of medical devices — Part 5: Tests for in vitro cytotoxicity, 2009.
[41] M. Kijanska, J. Kelm, In vitro 3D spheroids and microtissues: ATP-based cell viability and toxicity assays, Assay Guidance Manual in: G.A. Sittampalam GS, Brimacombe K, et al., (Ed.), Eli Lilly & Company and the National Center for Advancing Translational Sciences, Bethesda (MD), 2016.
[42] I.T. Ozbolat, Scaffold-based or scaffold-free bioprinting: competing or complementing approaches? J. Nanotechnol. Eng. Med. 6 (2) (2015).
[43] R. McMaster, C. Hoefner, A. Hrynevich, C. Blum, M. Wiesner, K. Wittmann, T.R. Dargaville, P. Bauer-Kreisel, J. Groll, P.D. Dalton, T. Blunk, Tailored melt electrowritten scaffolds for the generation of sheet-like tissue constructs from multicellular spheroids, Adv. Healthc. Mater. 8 (7) (2019) 1801326.
[44] G. Weisgrab, O. Guillaume, Z. Guo, P. Heimel, P. Slezak, A. Poot, D. Grijpma, A. Ovsianikov, 3D printing of large-scale and highly porous biodegradable tissue engineering scaffolds from poly(trimethylene-carbonate) using two-photon-polymerization, Biofabrication 12 (4) (2020) 045036.
[45] K. Alessandri, B.R. Sarangi, V.V. Gurchenkov, B. Sinha, T.R. Kießling, L. Fetler, F. Rico, S. Scheuring, C. Lamaze, A. Simon, S. Geraldo, D. Vignjević, H. Domé-jean, L. Rolland, A. Funfak, J. Bibette, N. Bremond, P. Nassoy, Cellular capsules as a tool for multicellular spheroid production and for investigating the mechanics of tumor progression in vitro, Proc. Natl. Acad. Sci. 110 (37) (2013) 14843–14848.
[46] K.C. Murphy, S.Y. Fang, J.K. Leach, Human mesenchymal stem cell spheroids in fibrin hydrogels exhibit improved cell survival and potential for bone healing, Cell Tissue Res. 357 (1) (2014) 91–99.
[47] K.C. Murphy, B.P. Hung, S. Browne-Bourne, D. Zhou, J. Yeung, D.C. Genetos, J.K. Leach, Measurement of oxygen tension within mesenchymal stem cell spheroids, J. R. Soc. Interface 14 (127) (2017).
[48] T.R. Olsen, B. Mattix, M. Casco, A. Herbst, C. Williams, A. Tarasidis, D. Simionescu, R.P. Visconti, F. Alexis, Manipulation of cellular spheroid composition and the effects on vascular tissue fusion, Acta Biomater. 13 (2015) 188–198.
[49] M. Stadler, M. Scherzer, S. Walter, S. Holzner, K. Pudelko, A. Riedl, C. Unger, N. Kramer, B. Weil, J. Neesen, M. Hengstschläger, H. Dolznig, Exclusion from spheroid formation identifies loss of essential cell-cell adhesion molecules in colon cancer cells, Sci. Rep. 8 (1) (2018) 1151.
[50] N.V. Kosheleva, Y.M. Efremov, B.S. Shavkuta, I.M. Zurina, D. Zhang, Y. Zhang, N.V. Minaev, A.A. Gorkun, S. Wei, A.A. Shpichka, I.N. Saburina, P.S. Timashev, Cell spheroid fusion: beyond liquid drops model, Sci. Rep. 10 (1) (2020) 12614.
[51] S. Žigon-Branc, M. Markovic, J. Van Hoorick, S. Van Vlierberghe, P. Dubruel, E. Zerobin, S. Baudis, A. Ovsianikov, Impact of hydrogel stiffness on differentiation of human adipose-derived stem cell microspheroids, Tissue Eng. Part A 25 (19-20) (2019) 1369–1380.
[52] E.V. Koudan, A.A. Gryadunova, P.A. Karalkin, J.V. Korneva, N.Y. Meteleva, I.I. Babichenko, A.V. Volkov, S.A. Rodionov, V.A. Parfenov, F.D.A.S. Pereira, Y.D. Khesuani, V.A. Mironov, E.A. Bulanova, Multiparametric analysis of tissue spheroids fabricated from different types of cells, Biotechnol. J. 15 (5) (2020) 1900217.